Optimized Design of Joint Mirror Array and Liquid Crystal-Based RIS-Aided VLC Systems

Omar Maraqa and Telex M. N. Ngatched, *Senior Member, IEEE*

***Abstract*—Most studies of reflecting intelligent surfaces (RISs)-assisted visible light communication (VLC) systems have focused on the integration of RISs in the channel to combat the line-of-sight (LoS) blockage and to enhance the corresponding achievable data rate. Some recent efforts have investigated the integration of liquid crystal (LC)-RIS in the VLC receiver to also improve the corresponding achievable data rate. To jointly benefit from the previously mentioned appealing capabilities of the RIS technology in both the channel and the receiver, in this work, we propose a novel indoor VLC system that is jointly assisted by a mirror array-based RIS in the channel and an LC-based RIS aided-VLC receiver. To illustrate the performance of the proposed system, a rate maximization problem is formulated, solved, and evaluated. This maximization problem jointly optimizes the roll and yaw angles of the mirror array-based RIS as well as the refractive index of the LC-based RIS VLC receiver. Moreover, this maximization problem considers practical assumptions, such as the presence of non-users blockers in the LoS path between the transmitter-receiver pair and the user's random device orientation (i.e., the user's self-blockage). Due to the non-convexity of the formulated optimization problem, a low-complexity algorithm is utilized to get the global optimal solution. A multi-user scenario of the proposed scheme is also presented. Furthermore, the energy efficiency of the proposed system is also investigated. Simulation results are provided, confirming that the proposed system yields a noteworthy improvement in data rate and energy efficiency performances compared to several baseline schemes.**

***Index Terms*—Reflecting intelligent surface (RIS), visible light communication (VLC), liquid crystals (LCs), random receiver orientation, achievable rate, energy efficiency (EE), line of sight (LoS) blockage.**

I. Introduction

THE exponential increase in connected devices and the ongoing development of wireless applications are driving the need to explore alternative wireless communications options to radio frequency (RF) communications. Visible light communications (VLC) has emerged as a bandwidth-abundant, cost-effective, and secure communications technology. Subsequently, VLC is seen as a promising candidate for complementing RF communications in future wireless networks [1].

Manuscript received 5 July 2023; accepted 9 July 2023. Date of publication 14 July 2023; date of current version 20 July 2023. This work was supported in part by the Natural Sciences and Engineering Research Council of Canada (NSERC) through its Discovery program, and in part by McMaster University. *(Corresponding author: Omar Maraqa.)*

The authors are with the Department of Electrical and Computer Engineering, McMaster University, Hamilton, ON L8S 4k1, Canada (e-mail: dr.omar.maraqa@gmail.com; ngatchet@mcmaster.ca).

Digital Object Identifier 10.1109/JPHOT.2023.3295350

In ordinary VLC systems, the line-of-sight (LoS) availability between the transmitter and the receiver is essential for reliable data transmission [2]. However, there may be other users (i.e., blockers) or obstacles that can obstruct this direct path, leading to LoS blockage which is common in indoor VLC systems [3]. The LoS path can also be blocked when the device orientation of the intended user is not aligned with the transmitter (i.e., self-blockage). Previous studies on VLC systems often assume that users' devices are facing upwards towards the ceiling (e.g., [3], [4], [5]), but in reality, users typically hold their devices in different positions. Research has shown that random device orientations do affect the quality and existence of LoS paths [6], so taking this into account is important when designing and analyzing VLC systems. Recently researchers have started unveiling the potential of integrating reflecting intelligent surfaces (RISs) on the walls to improve the communication links by reflecting waves from the transmitter toward the receiver. In case the LoS path is blocked, an RIS can reconfigure the wireless propagation channel to overcome this blockage. Accordingly, the adoption of RIS can relax the LoS requirement in VLC systems.

On the other hand, an ordinary VLC receiver typically includes a photo-detector (a photo-diode (PD), a photo-transistor, etc.), and a convex lens. In VLC systems, the incoming light must fall within the photo-detector's field-of-view (FoV) to recover the transmitted data successfully. To achieve this, convex lenses are used in ordinary VLC receivers as extent reducers to collect and focus the incoming light onto the photo-detector's active area. However, the use of a convex lens can lead to a reduction in the amount of incident light power of up to 30% because of reflection occurring at its top surface [7]. Additionally, convex lenses are not capable of dynamically steering the incoming light beam, which can limit the receiver's detection capabilities, especially with a large angle of incidence [8]. To overcome the aforementioned shortcoming of ordinary VLC receivers, Ndjiongue et al. [7] have proposed using voltage-controlled tunable liquid crystal (LC) in the receiver to adjust the direction of the incident light and to provide intensity amplification. Subsequently, this can enhance the strength of the received signal and increase the corresponding achievable data rate.

When it comes to the adoption of RIS in VLC systems, two main streams have evolved over the past few years, namely, (i) integrating a meta surface-based RIS [9], [10], [11], [12], [13], [14] or mirror array-based RIS [2], [15], [16], [17], [18], [19], [20], [21], [22], [23] on walls between the transmitter and the receiver (noting that the performance of the mirror array-based RIS outperforms the meta surface-based RIS [24]), and (ii)

incorporating an LC-based RIS in the receiver [8], [25], [26], [27] for light amplification and beam steering. However, to the best of the authors' knowledge, no one has investigated the joint benefit of integrating mirror array-based RIS on walls between the transmitter and the receiver and an LC-based RIS-aided receiver. Hence, this work intends to unveil the VLC system performance gain under such a joint design.

In this article, an indoor VLC system that jointly benefits from the RIS technology in both the channel and the receiver is proposed to overcome the LoS blockage problem that comes from both non-user blockers and self-blockage. The channel-assisted RIS improves the reliability of the VLC system, while the LC-based RIS-aided VLC receiver, with its amplification and light steering capabilities, enhances the strength of the received signal. The main contributions can be summarized as follows:

- A novel indoor VLC system that is jointly assisted by a mirror array-based RIS and an LC-based RIS-aided VLC receiver to enhance the corresponding achievable data rate is proposed. The proposed system takes into consideration the effects of non-user blockers and user's device orientation.
- A rate maximization problem for the proposed system that consists of a joint design of the roll and yaw angles of the mirror array-based RIS as well as the refractive index of the LC-based RIS-aided VLC receiver is formulated. Because the formulated multi-variate optimization problem is non-convex, a sine-cosine-based optimization algorithm is employed to obtain the global optimal solution.
- An additional scenario that considers the wall reflection with no RIS is analyzed and evaluated to illustrate the benefit of the integration of the RIS technology in improving the performance of VLC systems. Moreover, a multi-user scenario of the proposed scheme is presented, confirming that the proposed system yields a noteworthy improvement to VLC systems. Furthermore, an energy efficiency (EE) maximization problem for the proposed system is analyzed and solved because of the importance of this metric in evaluating VLC systems.
- Extensive simulation results are provided to illustrate the significant performance gains of the proposed joint system in terms of achievable data rate and EE when compared with several baseline schemes.

The structure of this article is as follows. The system and channel models of the proposed RIS-assisted VLC system that jointly consider both channel-assisted RIS and an LC-based RIS-aided receiver are presented in Section II. In Section III, the data rate optimization problem is formulated, and the sine-cosine-based optimization algorithm that gets the optimal solution for the formulated problem is presented. A scenario that considers the wall reflection with no RIS is presented in Section IV. In Section V, a multi-user scenario that utilizes the power domain non-orthogonal multiple access (NOMA) scheme is presented. The optimization of the energy efficiency metric (as an additional metric) for the proposed VLC system is provided in Section VI. Extensive simulation results are provided in Section VII, which is followed by the paper's conclusion and future research directions in Section VIII.

II. System and Channel Models

This section discusses the details of the indoor VLC environment, including the VLC system and channel models for the LoS path and the non-line-of-sight (NLoS) path resulting from the inclusion of the mirror array-based RIS in the channel, then the structure of the LC-based RIS-aided receiver with its light steering and amplification capabilities.

A. Indoor VLC Network

We consider an indoor downlink VLC system that is jointly assisted by a mirror array-based RIS and an LC-based RIS-aided VLC receiver as depicted in Fig. 1. In Fig. 1(a), the intended LoS path is denoted by a solid line and the RIS-assisted NLoS path is denoted by a dotted line. Also, multiple non-user blockers are randomly deployed in the system. If any of these blockers lies in the way of the LoS path, then the user would suffer from a signal outage. A signal outage might also occur if the user's device orientation is not perfectly aligned with the transmitter (i.e., user self-blockage). Hence, to overcome the outage from non-user blockers, an alternative path using the mirror array-based RIS is proposed. Additionally, to circumvent the outage from self-blockage, an LC-based RIS-aided receiver with light steering capability is proposed.

The orientation of the user's device is shown in Fig. 1(b), where the user can move his device in any direction, which can be determined by the device's azimuth angle, β, and the polar angle, α. The mirror array-based RIS is composed of several passive reflecting elements and deployed on a wall between the transmitter and the receiver. Fig. 1(c) and (d), show the orientation of an arbitrary element of the mirror array-based RIS with respect to the roll angle, ω, and the yaw angle, γ, respectively. Fig. 1(e) presents a schematic of an LC-based RIS-aided receiver, where an LC-based RIS module is placed in front of the PD. The LC-based RIS module is made up of a series of thin layers, within which tin oxide nano-disks that have LC infiltration are located, forming what is known as the LC cell. These layers include (i) an anti-reflection polarizer for filtering incoming light, (ii) a glass substrate to orient the LC molecules in a preferred direction, (iii) indium tin oxide for managing heat production and control, and (iv) a photo-alignment film that guides the light beam through the LC cell [7].

Fig. 1(f) illustrates how light propagates within the LC cell when an external voltage, v_{e}, exceeding the threshold voltage, v_{th}, is applied. The emitted light signal L_1 from the VLC AP travels through the air medium (from the mirror array-based RIS) with a refractive index η_a and reaches the interface between the air and the LC cell at an angle ξ. Since no light absorption occurs at this interface, a portion of the light signal L_1 is reflected while the remaining signal, L_2, is refracted at an angle θ as it passes through the LC cell, which has a thickness D and refractive index η_c. The electric field-induced molecular reorientation controls the propagation characteristics (such as direction and intensity) of the light signal as it passes through and exits the LC cell. This reorientation induces changes in the refractive index, η_c, enabling the LC RIS to control the wave-guiding capability primarily through the refractive index. Finally, Fig. 1(g) provides

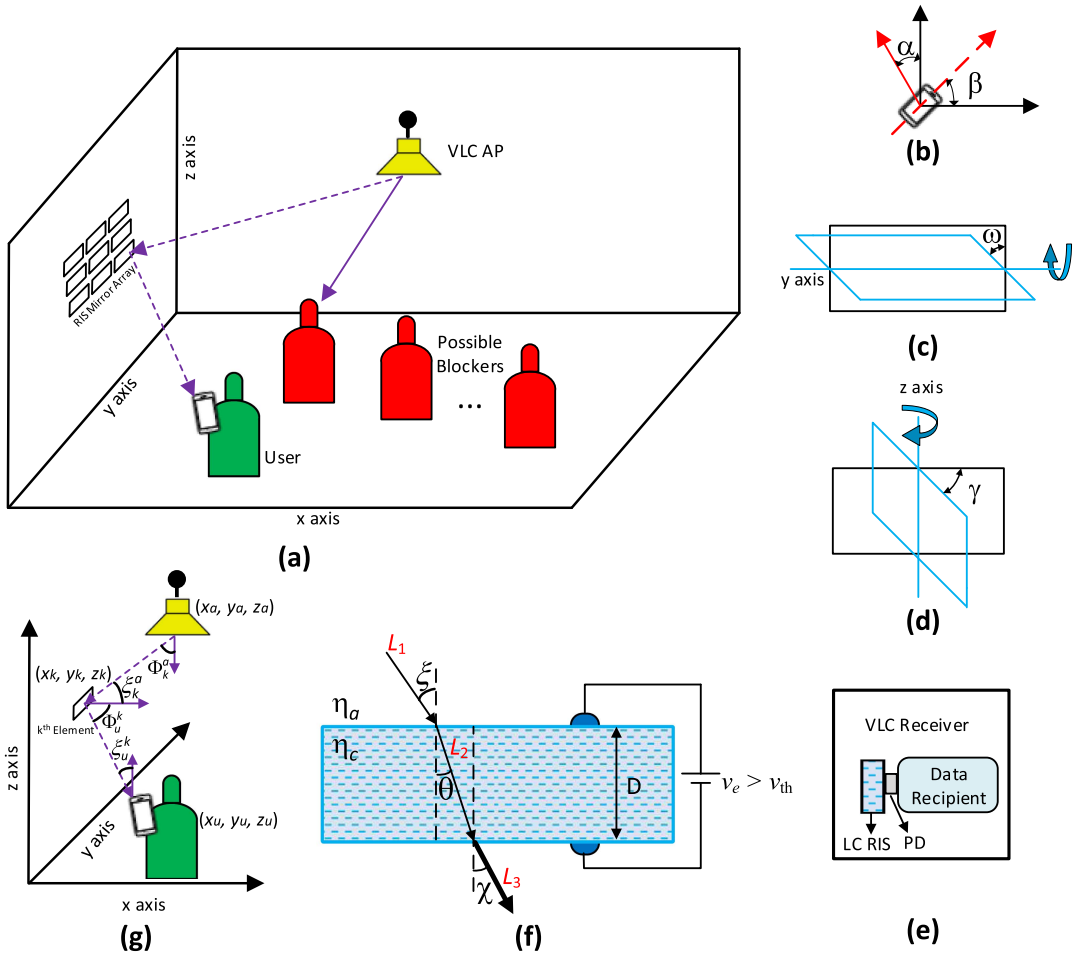

Fig. 1. Illustrations of the proposed joint mirror array and LC-based RIS-aided VLC system with random device orientation. (a) The proposed system with one VLC access point (AP), one user, a mirror array-based RIS, and non-user possible blockers, (b) the orientation of the user device with respect to the device's azimuth angle β and the device's polar angle α, (c) the orientation of the mirror array-based RIS with respect to the roll angle ω, (d) the orientation of the mirror array-based RIS with respect to the yaw angle γ, (e) a schematic of the LC-based RIS-aided receiver, (f) light signal propagation through the LC-based RIS-aided receiver, and (g) light signal propagation from the VLC AP (with a position vector (x_a, y_a, z_a)) to the intended user (with a position vector (x_u, y_u, z_u)) through the k-th element of the mirror array-based RIS (with a position vector (x_k, y_k, z_k)), while specifying the angles of irradiance and incidence of the light signal.

the angles of irradiance and incidence of the light signal starting from the VLC AP through the mirror array-based RIS to the intended user. The light signal irradiates from the VLC AP with an angle Φ_k^a, hits the mirror array-based RIS with an angle ξ_k^a, is reflected by the mirror array-based RIS with an angle Φ_u^k, and finally strikes the LC-based RIS surface with an angle ξ_u^k.

B. VLC Channel: Mirror Array-Based RIS

In the proposed VLC system, the channel model can be defined as the signal propagation through the air and the LC cell. The direct current (DC) gain represents the signal propagation through the air, while the transition coefficient represents the signal propagation through the LC cell. The gain of the channel between the AP and the user is expressed as [2]

$$H = \iota H_{\text{LoS}} \times \psi_{\text{LC-LoS}} + \sum_{k=1}^{\mathcal{K}} H_{\text{NLoS}}^{\text{RIS}_k} \times \psi_{\text{LC-NLoS}}, \quad (1)$$

where $\iota \in \{0, 1\}$ is an indicator function that represents whether or not the LoS path is obstructed. H_{LoS} denotes the channel gain of the LoS path, H_{NLoS} represents the NLoS channel gain, and $\psi_{\text{LC-LoS}}$ and $\psi_{\text{LC-NLoS}}$ denote the transition coefficient of the LoS and NLoS paths, respectively, which are discussed in Section II-C. $\mathcal{K}$ denotes the number of squared surfaces (i.e., elements) in the mirror array-based RIS. One can determine whether or not there is a reliable signal from the LoS path by examining if the received signal falls above the sensitivity of the photo-detector at the receiver. If the signal's strength is above the sensitivity of the photo-detector then I is set to one, otherwise, it is set to zero. For example, to achieve a bit-error-rate (BER) of less than 10^{-12}, the sensitivity of the photo-detector should be -35 dBm or above [28].

The channel gain for the LoS path is expressed as [29]

$$H_{\text{LoS}} = \begin{cases} \frac{(m+1)A_{\text{PD}}}{2\pi d^2} \cos^m(\Phi) \cos(\xi) G(\xi) T(\xi), \\ \qquad 0 \le \xi \le \xi_{\text{FoV}} \\ 0, \qquad \xi > \xi_{\text{FoV}}, \end{cases} \quad (2)$$

where m denotes the Lambertian index and is equal to $\frac{-1}{\log_2(\cos(\Phi_{1/2}))}$, with $\Phi_{1/2}$ as the semi-angle of the VLC AP,

A_{PD} denotes the physical area of the PD, d denotes the distance between the VLC AP and the intended user, Φ and ξ denote the angle of irradiance and angle of incidence, respectively, $T(\xi)$ denotes the gain of the optical filter, $G(\xi)$ denotes the gain of the optical concentrator, and $\xi_{\text{FoV}} \leq \frac{\pi}{2}$ denotes the PD's FoV. The gain of the optical concentrator is $G(\xi) = f^2/\sin^2 \xi_{\text{FoV}}$, $0 \leq \xi \leq \xi_{\text{FoV}}$, where f denotes the refractive index. The device's orientation highly influences the value of ξ, which can be expressed by both the azimuth and polar angles of the device as follows [30]

$$\begin{aligned}\cos(\xi) = &\left(\frac{x_a - x_u}{d}\right)\cos(\beta)\sin(\alpha)\\ &+\left(\frac{y_a - y_u}{d}\right)\sin(\beta)\sin(\alpha)\\ &+\left(\frac{z_a - z_u}{d}\right)\cos(\alpha),\end{aligned} \tag{3}$$

where (x_a, y_a, z_a) denotes the position vector of the VLC AP, and (x_u, y_u, z_u) the position vector of the user. The mirror array-based RIS is divided into $\mathcal{K}$ squared surfaces (i.e., elements), and each element has an area dA. In this article, similar to [2], [8], [24], we assume that the incoming optical signal from the AP hits the middle of the reflecting surfaces. The channel gain for the reflected signal from the k-th mirror array is obtained by [24]

$$H_{\text{NLoS}}^{\text{RIS}_k}(\gamma,\omega) = \begin{cases} \rho_{\text{RIS}} \frac{(m+1)A_{\text{PD}}}{2\pi^2 (d_k^a)^2 (d_u^k)^2} dA_k \cos^m(\Phi_k^a)\cos(\xi_k^a) \\ \quad \times \cos(\Phi_u^k)\cos(\xi_u^k) G(\xi) T(\xi), \\ \quad 0 \leq \xi_u^k \leq \xi_{\text{FoV}} \\ 0, \ \xi_u^k > \xi_{\text{FoV}}, \end{cases} \tag{4}$$

where ρ_{RIS} denotes the reflection coefficient of an RIS element, d_k^a represents the distance between the AP and the k-th reflecting element, d_u^k represents the distance between the k-th reflecting element and the intended user, dA_k is a reflective area of a small region, Φ_k^a is the irradiance angle from the AP toward the k-th reflecting element, ξ_k^a represents the incidence angle on the k-th reflecting element, Φ_u^k represents the irradiance angle from the k-th reflecting element towards the intended user, and ξ_u^k represents the incidence angle of the reflected signal at the user. The value of $\cos(\xi_u^k)$ can be obtained using (3), while the value of $\cos(\Phi_u^k)$ is given by [8]

$$\begin{aligned}\cos(\Phi_u^k) = &\left(\frac{x_k - x_u}{d_k^u}\right)\sin(\gamma)\cos(\omega)\\ &+\left(\frac{y_k - y_u}{d_k^u}\right)\cos(\gamma)\cos(\omega)\\ &+\left(\frac{z_k - z_u}{d_k^u}\right)\sin(\omega),\end{aligned} \tag{5}$$

where (x_k, y_k, z_k) denotes the position vector of the k-th reflecting element of the mirror array-based RIS.

C. LC-Based RIS-Aided Receiver: Amplification Gain and Light Steering

This subsection explains how the LC-based RIS module can enhance signal reception by amplifying and steering the incoming light, as shown in Fig. 1(f). This figure shows that the light intensity from the LC module at the refraction angle χ (labeled as L_3) is greater than the intensity of the incoming light, L_1. This light amplification occurs through stimulated emission, where photons from the incoming light interact with excited molecules in the LC module that have been stimulated by an external voltage, resulting in the creation of new, coherent photons. L_3 can be calculated using Beer's absorption law [31] and is given by

$$L3 = L1 \times \exp(\Gamma D) \times \psi_{\text{LC}}, \tag{6}$$

where $\exp(\Gamma D)$ represents the exponential increase in the intensity of the incident light, ψ_{LC} denotes the transition coefficient, and Γ symbolizes the amplification gain coefficient, which can be represented as [32]

$$\Gamma = \frac{2\pi\eta_c^3}{\lambda \cos(\xi_u^k)} r_{\text{eff}} E, \tag{7}$$

where λ denotes the wavelength of the optical signal, E, measured in [V/m], denotes the strength of the externally applied electric field, and r_{eff} denotes the electro-optic coefficient. From (7), it is evident that the amplification gain of the LC-based RIS is affected by the wavelength of the optical signal, the applied voltage, and the refractive index of the LC module. Therefore, it is crucial to choose these values thoughtfully to achieve the best possible performance of the LC-based RIS module.

The transition coefficient, ψ_{LC}, measures the effect of the LC-based RIS module on the total channel gain. It can be calculated by studying how light moves through the module as it enters, passes through the LC cell, and exits it. The transition coefficient of the NLoS path (i.e., the mirror array-based RIS path) can be expressed as follows [8]

$$\begin{aligned}\psi_{\text{LC-NLoS}} &= T_{\text{ac}}(\xi_u^k) \times T_{\text{ca}}(\theta)\\ &= (1 - R_{\text{ac}}(\xi_u^k)) \times (1 - R_{\text{ca}}(\theta)),\end{aligned} \tag{8}$$

where $T_{\text{ac}}(\xi_u^k)$ denotes the angular transmittance of the incident light on the interface between air and the LC cell and indicates how much of the incident light is refracted through it, $T_{\text{ca}}(\theta)$ denotes the angular transmittance as the light signal exits the LC cell. Since no light is absorbed in both the interface between air and the LC cell and at the interface between the LC cell and air (i.e., when the light signal enters and exits the LC cell, respectively), the light signal either gets reflected or refracted at these two interfaces. In (8), $R_{\text{ac}}(\xi_u^k)$ and $R_{\text{ca}}(\theta)$ represent the amount of light that gets reflected when the light signal enters or exits the LC cell, respectively. They can be expressed as follows [8]

$$R_{\text{ac}}(\xi_u^k) = \frac{1}{2}\left(\frac{\eta^2\cos(\xi_u^k) - \sqrt{\eta^2 - \sin^2(\xi_u^k)}}{\eta^2\cos(\xi_u^k) + \sqrt{\eta^2 - \sin^2(\xi_u^k)}}\right)^2$$

$$+\frac{1}{2}\left(\frac{\cos(\xi_u^k)-\sqrt{\eta^2-\sin^2(\xi_u^k)}}{\cos(\xi_u^k)+\sqrt{\eta^2-\sin^2(\xi_u^k)}}\right)^2, \quad (9)$$

$$R_{\text{ca}}(\theta)=\frac{1}{2}\left(\frac{\eta_1^2\cos(\theta)-\sqrt{\eta_1^2-\sin^2(\theta)}}{\eta_1^2\cos(\theta)+\sqrt{\eta_1^2-\sin^2(\theta)}}\right)^2 +\frac{1}{2}\left(\frac{\cos(\theta)-\sqrt{\eta_1^2-\sin^2(\theta)}}{\cos(\theta)+\sqrt{\eta_1^2-\sin^2(\theta)}}\right)^2, \quad (10)$$

where $\eta=\eta_c/\eta_a$ and $\eta_1=\eta_a/\eta_c$ denote the relative refractive indices when the light enters and exists the LC-based RIS, respectively, η_a and η_c are the refractive indices of the air medium and the LC cell, respectively. If the LoS path exists, (8) becomes $\psi_{\text{LC-LoS}}=T_{\text{ac}}(\xi_u^a)\times T_{\text{ca}}(\theta)$, where ξ_u^a represents the angle of incidence from the VLC AP on the LC-based RIS surface.

By examining (8) to (10), we can see that the transition coefficient can be optimized by adjusting the refractive index η_c of the LC-based RIS. This involves modifying the tilt angle ϕ, which determines the molecular orientation of the LC cell. The relation between the tilt angle and the refractive index is given by [33]

$$\frac{1}{\eta_c^2(\phi)}=\frac{\cos^2(\phi)}{\eta_e^2}+\frac{\sin^2(\phi)}{\eta_o^2}, \quad (11)$$

where $\eta_c(\phi)$ represents the refractive index of the LC cell at the specific tilt angle ϕ, η_e and η_o correspond to the extraordinary and ordinary refractive indices of the LC cell, respectively. It is worth noting that the tilt angle, ϕ, is controlled by an externally applied voltage, and the relationship between the two can be described as [8]

$$\phi=\begin{cases}\frac{\pi}{2}-2\tan^{-1}\left[\exp\left(-\frac{v_{\text{e}}-v_{\text{th}}}{v_0}\right)\right], & v_{\text{e}}>v_{\text{th}}\\ 0, & v_{\text{e}}\le v_{\text{th}}\end{cases} \quad (12)$$

where v_e refers to the externally applied voltage, v_{th} represents the critical voltage needed to initiate the tilting process, and v_0 is a fixed value. As the tilt angle, ϕ, is controlled by the voltage applied to the LC cell, according to (12), the LC cell can be utilized as a voltage-controlled RIS. This makes it possible to control the propagation of light by changing the refractive index, η_c, and refraction angle, ϕ, to steer the incoming light signal.

III. Achievable Data Rate Optimization

In this section, we present the details of the achievable data rate maximization problem investigated for the proposed joint mirror array and LC-based RIS-aided VLC system. Then, due to the non-convexity of the formulated multi-variate optimization problem, a sine-cosine-based optimization algorithm [34] is utilized to get the global optimal solution.

A. Achievable Data Rate Maximization Problem

The achievable data rate of the proposed system can be expressed by the following lower bound [35]

$$R_{\text{VLC}}=B\log_2\left(1+\frac{\exp(1)}{2\pi}\frac{\left(\frac{p}{q}R_{\text{PD}}\exp(\Gamma D)H\right)^2}{N_oB}\right), \quad (13)$$

where B denotes the system's bandwidth, p denotes the optical power, q represents the ratio of the electrical signal power to the optical transmit power, R_{PD} represents the responsivity of the PD, and N_o denotes the power spectral density of the noise. In order to maximize the rate, this article proposes (i) controlling the orientation of the mirror array by its roll angle, ω, and the yaw angle, γ, and (ii) adjusting the refractive index, η_c, of the LC-based module. With this, the achievable data rate maximization problem can be formulated as

$$\text{(P0)}: \max_{\{\omega,\gamma,\eta_c\}} \quad R_{\text{VLC}}, \quad (14)$$

$$\text{s.t.} \quad \text{C1}: -\frac{\pi}{2}\le\omega\le\frac{\pi}{2}, \quad (15)$$

$$\text{C2}: -\frac{\pi}{2}\le\gamma\le\frac{\pi}{2}, \quad (16)$$

$$\text{C3}: \ 1.5\le\eta_c\le 1.7, \quad (17)$$

where (15) and (16) represent the bounds of the roll angle and yaw angle, respectively. Constraint (17) represents the bounds of a typical off-the-shelf LC E7 (Merck) [36]. The above optimization problem is highly non-convex and cannot be solved using traditional optimization methods. Therefore, we utilize a metaheuristic approach based on the sine-cosine algorithm (SCA) [34] to find the appropriate orientation angles for the mirror array as well as the appropriate refractive index for the LC cell to achieve the best data rate performance. The SCA method was chosen over other metaheuristics due to its benefits, namely, its (i) ease of implementation, (ii) fast convergence, and (iii) ability to avoid local optimum solutions.

B. Proposed Solution Methodology

The SCA is a population-based stochastic optimization method introduced by Mirjalili in [34]. The method starts by generating random candidate solutions and gradually moves them toward the optimal solution using a mathematical model based on the sine and cosine functions. In the SCA method, at the beginning of each iteration, t, a set of search agents are randomly positioned within the feasible solution space of the optimization problem (P0). Each search agent represents a possible solution to the problem and its fitness is evaluated using the objective function (14). The agent with the highest fitness is selected as the destination point $\mathcal{D}^t$. In the next iteration $t+1$, each agent updates its solution using the following formula [34]

$$s_{n,v}^{t+1}=\begin{cases}s_{n,v}^t+r_1\times\cos(r_2)\times|r_3\mathcal{D}^t-s_{n,v}^t| & \text{if } r_4\ge 0.5,\\ s_{n,v}^t+r_1\times\sin(r_2)\times|r_3\mathcal{D}^t-s_{n,v}^t| & \text{if } r_4<0.5,\end{cases} \quad (18)$$

Algorithm 1: Proposed Solution Methodology for the Rate Maximization Problem in (P0).

Input: N, T, and a;
Output: The best solution $s_{n^*} = (\omega^*, \gamma^*, \eta_c^*)$, where n^* denotes an arbitrary search agent and $(\omega^*, \gamma^*, \eta_c^*)$ denotes the global optimal solution of (P0);

First Stage
Set $t = 0$;
Initialize the search agents with a set of random solutions $s_{n,\upsilon}^t$, $\forall n$;
Determine the fitness of each search agent using (13);
Store the solution of the fittest search agent in $\mathcal{D}^t$;
Second Stage
Set $t = 1$;
while *Termination criterion is not reached* **do**
  Get the value of the parameters: r_1,r_2, r_3, r_4;
  for $n = 1 : N$ **do**
    for $\upsilon = 1 : 3$ **do**
      Update the solutions $s_{n,\upsilon}^t$, $\forall n$ using (18);
    end
  end
  Check for search agents that violate the constraints of (P0) and remove the violations to guarantee the solutions' feasibility;
  Update the fitness of each search agent using (13);
  Update $\mathcal{D}^t$ if there is any better solution;
  Update the iteration counter $t = t + 1$;
end
return $s_{n^*} = (\omega^*, \gamma^*, \eta_c^*)$;

where $s_{n,\upsilon}^t$ refers to the solution of the n-th agent at the t-th iteration, while $s_{n,\upsilon}^{t+1}$ represents the current updated solution, and the symbol $|.|$ means the absolute value of the expression enclosed in it. The parameters r_1, r_2, r_3, and r_4 can be expressed as follows. $r_1 = a - t\frac{a}{T}$, where T is a predefined maximum iteration number and a is a constant value. Depending on the value of the randomly generated parameter r_1, the movement direction for the current agent could be towards (if $r_1 < 1$) or away from (if $r_1 > 1$) the destination point. The parameter r_2 controls how far the movement should be towards or away from the destination point and its value is randomly chosen in the interval $(0, 2\pi)$. The parameter r_3 determines how much the destination point affects the distance between the current solution and the destination point and its value is randomly chosen through uniform random distribution in the interval (0,2). Finally, the parameter r_4 that falls in the interval (0,1) switches randomly between the cosine and sine components. In (18), $r_1 \times \cos(r_2)$ and $r_1 \times \sin(r_2)$ enables both exploration and exploitation during the search process. In particular, when these two values are greater than 1 or less than -1, the algorithm conducts a global exploration search. Conversely, when these two values fall within the range of -1 to 1, the algorithm performs an exploitation search. The algorithm guides agents toward the best-known positions in the search space and updates their solutions until a maximum number of iterations (i.e., a termination criterion) is reached. A summary of the proposed solution methodology for the rate maximization problem in (P0) is provided in Algorithm 1. This article assumes that Algorithm 1 is implemented by a central control unit, linked to both the RIS mirrors and the AP, which is capable of acquiring the necessary downlink channel state information.

C. Computational Complexity Analysis

The computational complexity of Algorithm 1 can be evaluated as follows. At first, the generation of the initial set of solutions for all agents necessitates $\mathcal{O}(NV)$ operations, where N and V are the numbers of search agents and decision variables, respectively. The process of evaluating the solution fitness for all agents needs $\mathcal{O}(N)$ operations, and selecting the destination point has a complexity of $\mathcal{O}(N)$. As a result, the first-stage computational complexity of Algorithm 1 is $\mathcal{O}(NV)$. The worst-case complexity for updating the solution sets based on (18) is $\mathcal{O}(NVT)$. The worst-case complexity for evaluating the updated solution fitness for all agents is $\mathcal{O}(NT)$, and is $\mathcal{O}(NT)$ for updating the destination point. Thus, the second-stage worst-case computational complexity of Algorithm 1 is $\mathcal{O}(NVT)$. Therefore, based on the aforementioned discussion, the overall worst-case computational complexity for finding a solution using Algorithm 1 is approximately $\mathcal{O}(NVT)$, which consists of the $\mathcal{O}(NV)$ complexity of the first stage and the $\mathcal{O}(NVT)$ complexity of the second stage.

IV. Wall Reflection's Scenario

In this section, we examine the scenario with no RIS, but where the wall's reflection paths are considered. We only take into account first-order reflection since, as demonstrated in [3], the performance of VLC systems is minimally affected by higher-order reflections. The channel gain of the first-order reflection from the wall surface is expressed as [29]

$$H_{\text{NLoS}}^{\text{wall}} = \begin{cases} \rho_{\text{wall}} \frac{(m+1)A_{\text{PD}}}{2\pi^2 (d_w^a)^2 (d_u^w)^2} dA_k \cos^m(\Phi_w^a) \cos(\xi_w^a) \cos(\Phi_u^w) \\ \quad \times \cos(\xi_u^w) G(\xi) T(\xi), \ 0 \le \xi_u^w \le \xi_{\text{FoV}} \\ 0, \qquad\qquad\qquad\qquad\qquad \xi_u^w > \xi_{\text{FoV}} \end{cases} \tag{19}$$

where ρ_{wall} denotes the wall's surface reflection coefficient.

The achievable rate of this proposed scenario can be expressed by the lower bound [35]

$$R_{\text{VLC}}^{\text{wall}} = B\log_2 \left(1 + \frac{\exp(1)}{2\pi} \times \frac{\left(\frac{p}{q} R_{\text{PD}} \exp(\Gamma D) \left(\iota H_{\text{LoS}} \psi_{\text{LC-LoS}} + H_{\text{NLoS}}^{\text{wall}} \psi_{\text{LC-NLoS}} \right) \right)^2}{N_o B} \right). \tag{20}$$

To maximize the achievable rate of this scenario, we replace the objective function of (P0) by (20), and solve the resultant optimization problem by following the same steps mentioned in Section III-B.

V. Multi-User Scenario

To implement this scenario, we assume that the number of intended users is U and these users are sorted based on their channel gain $H_1 \le H_2 \le \ldots \le H_U$ [37]. Also, we utilize the power domain NOMA scheme to serve these users. According to

the NOMA scheme, the VLC AP transmits a superposed signal, x, to serve the intended users, which can be represented as [38]

$$x = \left(\sum_{u=1}^{U} \sqrt{c_u P_{\mathrm{S}}} s_u \right) + I_{\mathrm{DC}}, \tag{21}$$

where c_u and s_u denote the allocated power ratio and the modulated message signal intended for the u-th user, respectively. P_{S} is the electrical transmit power of the signal, which is equal to $(\frac{p}{q})^2$. I_{DC} is a fixed bias current added to ensure the positive instantaneous intensity [37]. Based on [38], c_u can be expressed as

$$c_u = \begin{cases} \zeta(1-\zeta)^{u-1}, & \text{if } 1 \leq u < U \\ (1-\zeta)^{u-1}, & \text{if } u = U \end{cases} \tag{22}$$

where ζ is a fixed value in the range (0.5,1] and $\sum_{u=1}^{U} c_u = 1$. The received signal at the u-th user, after removing the DC bias, is given by [38]

$$y_u = H_u \times \left(\sum_{u=1}^{U} \sqrt{c_u P_{\mathrm{S}}} s_u \right) + z_u, \tag{23}$$

where z_u symbolizes the additive real-valued Gaussian noise with variance σ^2 (i.e., $z_u \sim \mathcal{N}(0, \sigma^2)$), which includes both the thermal and shot noises. According to the NOMA scheme, each user needs to perform successive interference cancellation (SIC) to decode its information [39]. For simplicity, we assume that there is no residual interference after performing the SIC process (i.e., perfect SIC) [40]. Accordingly, the sum rate of the proposed system can be expressed as

$$R_{\mathrm{sum}} = \sum_{u=1}^{U} R_u,$$

where

$$R_u = \begin{cases} B\log_2\left(1 + \frac{\exp(1)}{2\pi} \frac{(R_{\mathrm{PD}}\exp(\Gamma D) H_u)^2 c_u P_{\mathrm{S}}}{I + N_o B}\right), 1 \leq u < U \\ B\log_2\left(1 + \frac{\exp(1)}{2\pi} \frac{(R_{\mathrm{PD}}\exp(\Gamma D) H_u)^2 c_u P_{\mathrm{S}}}{N_o B}\right), u = U \end{cases} \tag{24}$$

and $I = \sum_{i=u+1}^{U} (R_{\mathrm{PD}}\exp(\Gamma D) H_u)^2 c_i P_{\mathrm{S}}$ represents the inter-user interference term resulting from the application of the NOMA scheme. To maximize the sum rate metric of this scenario, we replace the objective function of (P0) by (24), and solve the resultant optimization problem by following the same steps mentioned in Section III-B.

VI. Energy Efficiency Optimization

The EE has become a widely used performance metric in VLC systems [10], [41], [42], [43]. The EE can be defined as the "ratio between the VLC system's achievable rate and the total consumed power" and is expressed in Bits/Joule [41]. The achievable rate of the proposed system is provided in (13). The total consumed power of the proposed system includes, the power consumed at the transmitter, RIS, and receiver. The consumed power at the transmitter mainly involves the power consumption of the signal power, digital to analog converter (DAC), filter, power amplifier, light emitting diode (LED) driver, and transmitter external circuit. The consumed power at the mirror array-based RIS only includes the power required to rotate all the elements of the mirror array, since the mirrors are passive elements. Lastly, the consumed power at the receiver mainly involves the power consumption of analog to digital converter (ADC), trans-impedance amplifier (TIA), filter, LC, and receiver external circuit. Accordingly, the total power consumption of the proposed system is described by [42], [43]

$$\begin{aligned} P_{\mathrm{total}} &= P_{\mathrm{T}} + P_{\mathrm{RIS}} + P_{\mathrm{R}}, \\ P_{\mathrm{T}} &= P_{\mathrm{S}} + P_{\mathrm{DAC}} + P_{\mathrm{Filter}} + P_{\mathrm{PA}} + P_{\mathrm{Driver}} + P_{\mathrm{T\text{-}Circuit}}, \\ P_{\mathrm{RIS}} &= P_{\mathrm{m}} \times \mathcal{K}, \\ P_{\mathrm{R}} &= P_{\mathrm{ADC}} + P_{\mathrm{TIA}} + P_{\mathrm{Filter}} + P_{\mathrm{LC}} + P_{\mathrm{R\text{-}Circuit}}, \end{aligned} \tag{25}$$

where the power consumption parameters mentioned in (25) can be quoted from the data sheets of VLC systems. According to the previous analysis, the EE of the proposed system can be expressed as

$$\mathrm{EE} = \frac{R_{\mathrm{VLC}}}{P_{\mathrm{total}}}. \tag{26}$$

To maximize the EE metric, we replace the objective function of (P0) by (26), and solve the resultant optimization problem by following the same steps mentioned in Section III-B.

TABLE I
Simulation Parameters

Parameter	Value	Parameter	Value
$\Phi_{1/2}$	70°	A_{PD}	1.0 cm^2
d	2.5 m	$T(\xi)$	1.0
ξ_{FoV}	85°	f	1.5
ρ_{wall}	0.8	ρ_{RIS}	0.95
η_a	1.0	η_e	1.7
η_o	1.5	v_{th}	1.34 V
v_0	1.0 V	D	0.75 mm
λ	$\{510, 670\}$ nm	r_{eff}	12 pm/V
B	200 MHz	q	3.0
R_{PD}	0.53 A/W	N_o	$10^{-21}\mathrm{A}^2/\mathrm{Hz}$
N	2	V	3
a	2.0	T	400
P_{DAC}	175 mWatt	P_{ADC}	95 mWatt
P_{Filter}	2.5 mWatt	P_{Driver}	2758 mWatt
P_{TIA}	2500 mWatt	P_{m}	100 mWatt
$P_{\mathrm{T\text{-}Circuit}}$	3250 mWatt	$P_{\mathrm{R\text{-}Circuit}}$	1.9 mWatt
P_{PA}	280 mWatt	P_{LC}	320 mWatt

VII. Simulation Results

In this section, we present detailed numerical results to evaluate the performance of the proposed joint mirror array and LC-based RIS-aided VLC system. A list of the default parameters used in this section is provided in Table I. Beyond this list, based on the findings presented in [30], the azimuth angle, β, follows a uniform distribution with a value ranging in the interval $[-\pi, \pi]$. On the other hand, the polar angle, α, can be described by using the Laplace distribution with a mean of

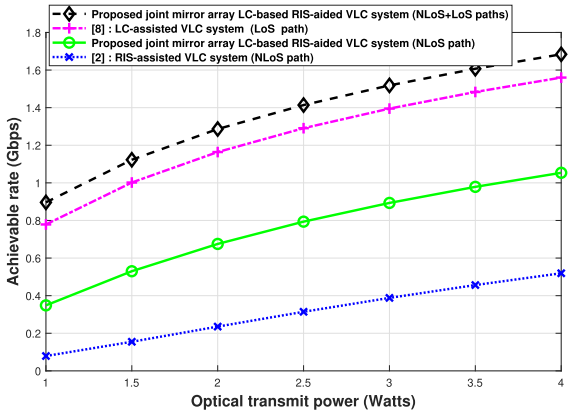

Fig. 2. The achievable data rate performance of the proposed joint mirror array LC-based RIS-aided VLC system with both a NLoS-path case and a NLoS-plus-LoS-paths case compared to the following counterparts: (i) LC-based RIS-aided VLC system [8] with a LoS path, and (ii) RIS-assisted VLC system [2] with a NLoS path. At $\lambda = 510$ nm.

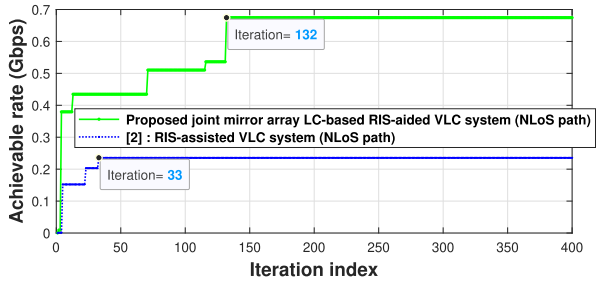

Fig. 3. The convergence curves of the SCA algorithm for the proposed joint mirror array LC-based RIS-aided VLC system compared to its counterpart of RIS-assisted VLC system [2]. At $p = 2$ Watts and $\lambda = 510$ nm.

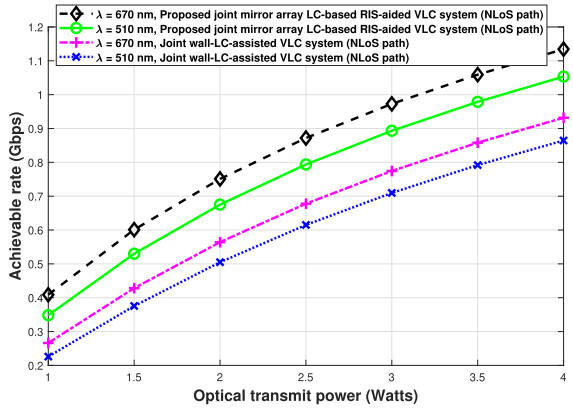

Fig. 4. The achievable data rate performance of the proposed joint mirror array LC-based RIS-aided VLC system compared to its counterpart of wall-LC-assisted VLC system (mentioned in Section IV) for light signals of different wavelengths.

41 degrees and a standard deviation of 9 degrees. The polar angle is typically within the range of $[0, \frac{\pi}{2}]$. The users in the system are represented as cylinders that have a radius of 0.15 meters and a height of 1.65 meters. The receiver is held by a user who is positioned at 0.85 meters above the ground and 0.36 meters away from the user's body. The mirror array-based RIS consists of 10 rows and 30 columns of mirrors, with each mirror measuring 0.1 meters by 0.1 meters. Both the dimension of the considered mirror array-based RIS (in the y-z plane) and the dimension of the wall of interest (in the x-z plane) is $1.0\ \text{m} \times 3.0\ \text{m}$. The room size is $5.0\ \text{m} \times 5.0\ \text{m} \times 3.0\ \text{m}$ and the VLC AP is positioned at the center of the room ceiling with a position vector $2.5\ \text{m} \times 2.5\ \text{m} \times 3.0\ \text{m}$. In the simulation of the NLoS scenario, we set I to zero. All the parameters used in this section are quoted from [2], [8], [38], [40], [42], [43].

Fig. 2 compares the achievable data rate performance of the proposed joint mirror array LC-based RIS-aided VLC system with both a NLoS-path case and a NLoS-plus-LoS-paths case to the following counterparts: (i) LC-based RIS-aided VLC system with a LoS path [8], and (ii) RIS-assisted VLC system with a NLoS path [2]. It can be observed that, when both the LoS and NLoS paths are considered, the proposed system achieves up to 115% improvement in the data rate performance compared to the counterpart in (i). Also, when the LoS path is obstructed, the proposed system achieves up to 404% improvement in the data rate performance compared to the counterpart in (ii). This illustrates that adopting the RIS technology in both the channel and at the receiver contribute to a significant enhancement of the VLC system's achievable data rate.

Fig. 3 shows a convergence analysis of the SCA algorithm for the proposed system compared to its counterpart of RIS-assisted VLC system. In this figure, the proposed joint mirror array LC-based RIS-aided VLC system needs around 4 times more iterations to converge to the global optimal solution, compared to its counterpart of RIS-assisted VLC system. This behavior is expected since the proposed system has a larger search space compared to its counterpart. Specifically, according to the analysis provided in Section III-C and the simulation parameters in Table I, one can deduce that the search space (i.e., the overall worst-case computational complexity that is equal $\mathcal{O}(NVT)$) for the proposed system is double the search space of the RIS-assisted counterpart.

Fig. 4 compares the achievable data rate performance of the proposed joint mirror array LC-based RIS-aided VLC system to its counterpart of wall-LC-assisted VLC system (mentioned in Section IV) for light signals of different wavelengths. This figure is simulated for different wavelengths since changing the wavelengths influences the data rate performance of the LC-based RIS-aided receiver. In this figure, changing the wavelength of the light signals from 510 nm to 670 nm achieves up to 117% and 118% improvement in the data rate performance for the proposed joint mirror array LC-based RIS-aided VLC system and wall-LC-assisted VLC system, respectively. Additionally, the proposed joint mirror array LC-based RIS-aided VLC system achieves up to 154% improvement in the data rate performance compared to its counterpart of wall-LC-assisted VLC system. This demonstrates how pivotal the integration of the RIS technology is in improving the performance of VLC systems.

Fig. 5 compares the sum rate performance of the multi-user scenario (mentioned in Section V) for the proposed joint mirror array LC-based RIS-aided VLC system to its counterpart of RIS-assisted VLC system. In this figure, the provided sum rate results for the multi-user case shows a similar trend compared

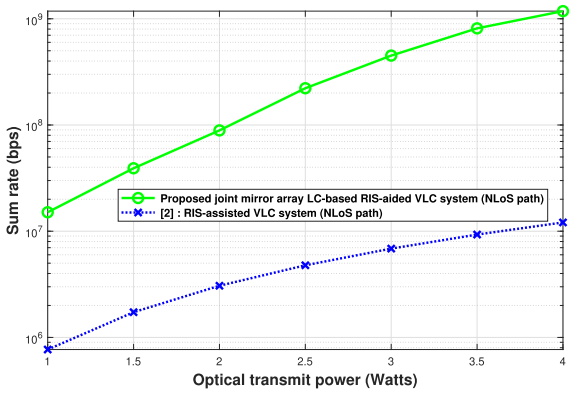

Fig. 5. The sum rate performance of the proposed joint mirror array LC-based RIS-aided VLC system compared to its counterpart of RIS-assisted VLC system [2]. At $\lambda = 510$ nm, $\zeta = 0.6$, and $U = 4$.

to the single intended user case (e.g., see Fig. 2), where the proposed system achieves up to 196% improvement in the data rate performance compared to the counterpart in [2]. Also, if we compare the sum rate performance of the multi-user case, in this figure, with the rate performance of the single intended user case reported in Fig. 2, we can notice some rate performance degradation here. Such a trend is expected for two reasons, (i) in the adopted multi-user scenario, the NOMA scheme is utilized to serve the intended users simultaneously at the expense of introducing an inter-user interference that deteriorates the rate performance of the VLC system, and (ii) in the adopted multi-user scenario, the optical transmit power of the VLC AP is divided between the intended users (as explained in (22)).

Fig. 6 compares the achievable data rate, consumed-power, and energy efficiency performance of the proposed joint mirror array LC-based RIS-aided VLC system compared to its counterpart of RIS-assisted VLC system [2] for a different number of elements in the mirror array-based RIS. In Fig. 6(a), one can see that the achievable data rate performance of the proposed system increases steadily and then starts to saturate when the number of elements in the mirror array-based RIS increases. This is because adding extra elements in a large mirror array-based RIS provides marginal gain. A similar trend has been reported in [9], [20]. Fig. 6(b) shows that the total power consumption of the proposed system is slightly higher than its counterpart of RIS-assisted VLC system. The extra power consumption comes from the inclusion of the LC-based RIS module in the VLC receiver. From Fig. 6(c), three main observations can be deduced, (i) as the number of elements in the mirror array-based RIS increases the system's EE increases then decreases. Such a trend in the system can be justified by the following argument: the increase in the number of elements is reflected as a logarithmic increase in the system's achievable data rate (Fig. 6(a)) and as a linear increase in the total power consumption of the proposed system (Fig. 6(b)). (ii) Although the proposed system consumes more power compared to its counterpart of RIS-assisted VLC system, it achieves up to 284% improvement in the overall EE performance. (iii) In our proposed system, the best EE performance is obtained when the number of elements in the mirror array-based RIS is one hundred. At this point, the proposed

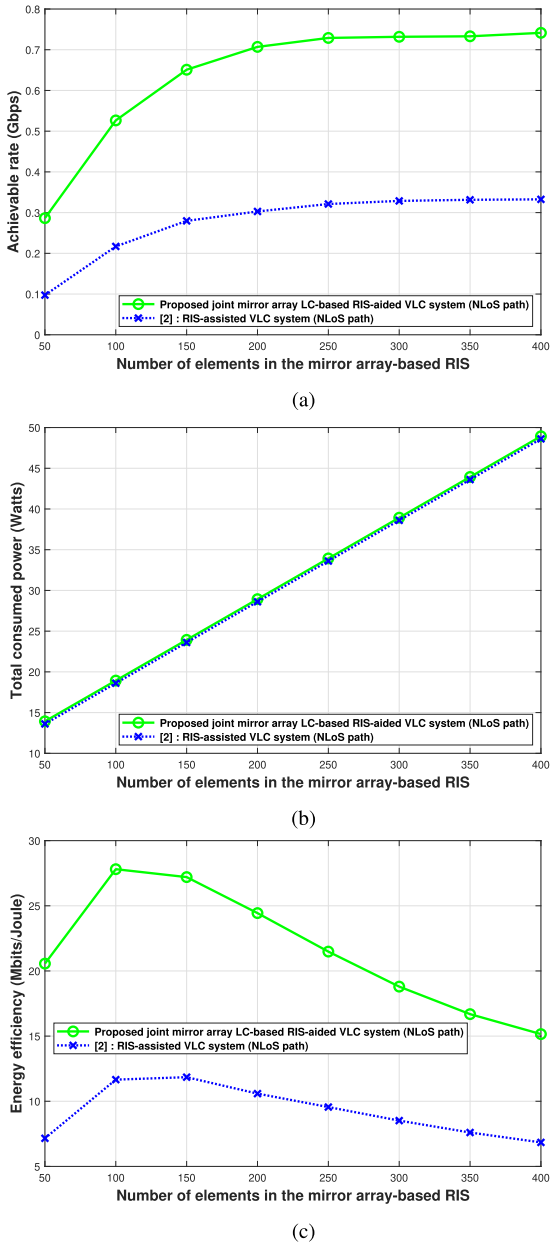

Fig. 6. (a) The achievable data rate, (b) consumed-power, and (c) energy efficiency performance of the proposed joint mirror array LC-based RIS-aided VLC system compared to its counterpart of RIS-assisted VLC system [2] for a different number of elements in the RIS mirror array. At $p = 2$ Watts and $\lambda = 510$ nm.

VLC system achieves a good trade-off between the achievable rate improvement and the total consumed power. Fig. 6(c) is obtained by replacing the objective function of (P0) by (26) and then optimizing the EE metric by following the same steps mentioned in Section III-B.

VIII. Conclusion and Future Research Directions

In this article, a novel indoor VLC system that is jointly assisted by a mirror array-based RIS and an LC-based RIS-aided VLC receiver to enhance the corresponding achievable data rate is presented and investigated. The proposed system combats

the LoS blockage that results from (i) non-user blockers and (ii) the user's device orientation (i.e., self-blockage). A rate maximization problem and an EE maximization problem are formulated, solved, and evaluated for the proposed system. These maximization problems jointly optimize the roll and yaw angles of the mirror array-based RIS as well as the refractive index of the LC-based RIS-aided VLC receiver. Because the formulated multi-variate optimization problems are non-convex, a sine-cosine-based optimization algorithm is employed to obtain the global optimal solution for both problems with very low complexity. Simulation results have revealed that adopting such joint mirror array LC-based RIS-aided deployment can dramatically improve the data rate as well as the EE of indoor VLC systems when compared to baselines of considering (i) only a mirror array-based RIS, and (ii) a wall-LC-assisted VLC system. Also, the proposed deployment reveals that it is possible to improve the data rate and the energy efficiency of VLC systems without using additional bandwidth resources and transmit power.

Some interesting future research areas include, (i) extending the proposed system to a hybrid RF/optical wireless communications (OWC), where RF communications can be utilized in the uplink to support a complete uplink-downlink system, (ii) extending the proposed system to a multiple APs deployment with multi-users, while considering a static/dynamic RIS configuration [44], (iii) investigating the use of a laser diode (LD) instead of the white LED used in the proposed system, (iv) validating the proposed theoretical system using an experimental test-bed, and (v) considering the illumination constraints and the human factors of the proposed VLC system.

REFERENCES

[1] S. Al-Ahmadi, O. Maraqa, M. Uysal, and S. M. Sait, "Multi-user visible light communications: State-of-the-art and future directions," *IEEE Access*, vol. 6, pp. 70555–70571, 2018.

[2] S. Aboagye, T. M. N. Ngatched, O. A. Dobre, and A. R. Ndjiongue, "Intelligent reflecting surface-aided indoor visible light communication systems," *IEEE Commun. Lett.*, vol. 25, no. 12, pp. 3913–3917, Dec. 2021.

[3] T. Tang, T. Shang, and Q. Li, "Impact of multiple shadows on visible light communication channel," *IEEE Commun. Lett.*, vol. 25, no. 2, pp. 513–517, Feb. 2021.

[4] S. Aboagye, A. Ibrahim, T. M. N. Ngatched, A. R. Ndjiongue, and O. A. Dobre, "Design of energy efficient hybrid VLC/RF/PLC communication system for indoor networks," *IEEE Wireless Commun. Lett.*, vol. 9, no. 2, pp. 143–147, Feb. 2020.

[5] S. Aboagye, T. M. N. Ngatched, O. A. Dobre, and A. Ibrahim, "Joint access point assignment and power allocation in multi-tier hybrid RF/VLC HetNets," *IEEE Trans. Wireless Commun.*, vol. 20, no. 10, pp. 6329–6342, Oct. 2021.

[6] Y. S. Eroglu, Y. Yapici, and I. Guvenc, "Impact of random receiver orientation on visible light communications channel," *IEEE Trans. Commun.*, vol. 67, no. 2, pp. 1313–1325, Feb. 2019.

[7] A. R. Ndjiongue, T. M. Ngatched, O. A. Dobre, and H. Haas, "Reconfigurable intelligent surface-based VLC receivers using tunable liquid-crystals: The concept," *J. Light. Technol.*, vol. 39, no. 10, pp. 3193–3200, May 2021.

[8] S. Aboagye, A. R. Ndjiongue, T. M. N. Ngatched, and O. A. Dobre, "Design and optimization of liquid crystal RIS-based visible light communication receivers," *IEEE Photon. J.*, vol. 14, no. 6, Dec. 2022, Art. no. 7355607.

[9] S. Sun, W. Mei, F. Yang, N. An, J. Song, and R. Zhang, "Optical intelligent reflecting surface assisted MIMO VLC: Channel modeling and capacity characterization," Feb. 2023, *arXiv:2302.03893*.

[10] B. Cao, M. Chen, Z. Yang, M. Zhang, J. Zhao, and M. Chen, "Reflecting the light: Energy efficient visible light communication with reconfigurable intelligent surface," in *Proc. IEEE Veh. Technol. Conf.*, 2020, pp. 1–5.

[11] A. Salehiyan and M. J. Emadi, "Performance analysis of uplink optical wireless communications in the presence of a simultaneously transmitting and reflecting reconfigurable intelligent surface," *IET Optoelectron.*, early access, May 2023.

[12] C. Liu, L. Yu, X. Yu, J. Qian, Y. Wang, and Z. Wang, "Capacity analysis of RIS-assisted visible light communication systems with hybrid NOMA," in *Proc. IEEE Glob. Commun.*, 2022, pp. 118–123.

[13] H. Abumarshoud, B. Selim, M. Tatipamula, and H. Haas, "Intelligent reflecting surfaces for enhanced NOMA-based visible light communications," in *Proc. IEEE Int. Conf. Commun.*, 2022, pp. 571–576.

[14] Z. Liu, F. Yang, S. Sun, J. Song, and Z. Han, "Sum rate maximization for NOMA-based VLC with optical intelligent reflecting surface," *IEEE Wireless Commun. Lett.*, vol. 12, no. 5, pp. 848–852, May 2023.

[15] S. Sun, F. Yang, and J. Song, "Sum rate maximization for intelligent reflecting surface-aided visible light communications," *IEEE Commun. Lett.*, vol. 25, no. 11, pp. 3619–3623, Nov. 2021.

[16] L. Qian, X. Chi, L. Zhao, and A. Chaaban, "Secure visible light communications via intelligent reflecting surfaces," in *Proc. IEEE Int. Conf. Commun.*, 2021, pp. 1–6.

[17] H. Abumarshoud, C. Chen, I. Tavakkolnia, H. Haas, and M. A. Imran, "Intelligent reflecting surfaces for enhanced physical layer security in NOMA VLC systems," Nov. 2022, *arXiv:2211.09456*.

[18] S. Sun, F. Yang, J. Song, and Z. Han, "Joint resource management for intelligent reflecting surface–aided visible light communications," *IEEE Trans. Wireless Commun.*, vol. 21, no. 8, pp. 6508–6522, Aug. 2022.

[19] S. Sun, F. Yang, J. Song, and R. Zhang, "Intelligent reflecting surface for MIMO VLC: Joint design of surface configuration and transceiver signal processing," *IEEE Trans. Wireless Commun.*, early access, Jan. 2023, doi: 10.1109/TWC.2023.3236811.

[20] Q. Wu, J. Zhang, Y. Zhang, G. Xin, and J. Guo, "Configuring reconfigurable intelligent surface for parallel MIMO visible light communications with asymptotic capacity maximization," *Appl. Sci.*, vol. 13, no. 1, Dec. 2022, Art. no. 563.

[21] X.-D. Shi, L.-H. Hong, P.-F. Yu, J.-W. Shi, N. Liu, and J.-Y. Wang, "Performance analysis and parameter optimization for intelligent reflecting mirror array-aided visible light communications," *J. Opt. Soc. Amer. A*, vol. 39, no. 10, pp. 1839–1848, Oct. 2022.

[22] T. Yang et al., "Average signal-to-noise ratio maximization for an intelligent reflecting surface and angle diversity receiver jointly assisted indoor visible light communication system," *Appl. Opt.*, vol. 61, no. 35, pp. 10390–10399, Dec. 2022.

[23] D. A. Saifaldeen, B. S. Ciftler, M. M. Abdallah, and K. A. Qaraqe, "DRL-based IRS-assisted secure visible light communications," *IEEE Photon. J.*, vol. 14, no. 6, Dec. 2022, Art. no. 8656209.

[24] A. M. Abdelhady, A. K. S. Salem, O. Amin, B. Shihada, and M.-S. Alouini, "Visible light communications via intelligent reflecting surfaces: Metasurfaces vs mirror arrays," *IEEE Open J. Commun. Soc.*, vol. 2, pp. 1–20, 2021.

[25] A. Krohn, A. Harlakin, S. Arms, S. Pachnicke, and P. A. Hoeher, "Impact of liquid crystal based interference mitigation and precoding on the multiuser performance of VLC massive MIMO arrays," *IEEE Photon. J.*, vol. 14, no. 5, Oct. 2022, Art. no. 7348112.

[26] A. Krohn, S. Pachnicke, and P. A. Hoeher, "Genetic optimization of liquid crystal matrix based interference suppression for VLC MIMO transmissions," *IEEE Photon. J.*, vol. 14, no. 1, Feb. 2022, Art. no. 7300705.

[27] Q. Wu, J. Zhang, Y. Zhang, G. Xin, and D. Guo, "Asymptotic capacity maximization for MISO visible light communication systems with a liquid crystal RIS-based receiver," *Photonics*, vol. 10, no. 2, Jan. 2023, Art. no. 128.

[28] R. Hui and M. O'Sullivan, *Fiber-Optic Measurement Techniques*. London, U.K.: Academic Press, 2022.

[29] T. Komine and M. Nakagawa, "Fundamental analysis for visible-light communication system using LED lights," *IEEE Trans. Consum. Electron.*, vol. 50, no. 1, pp. 100–107, Feb. 2004.

[30] M. D. Soltani, A. A. Purwita, Z. Zeng, H. Haas, and M. Safari, "Modeling the random orientation of mobile devices: Measurement, analysis and LiFi use case," *IEEE Trans. Commun.*, vol. 67, no. 3, pp. 2157–2172, Mar. 2019.

[31] W. Demtröder, *Laser Spectroscopy 1: Basic Principles*. Berlin, Germany: Springer, 2014.

[32] V. Marinova, S. Huei Lin, R. Chung Liu, and K. Y. Hsu, "Photorefractive effect: Principles, materials, and near-infrared holography," *Wiley Encyclopedia of Electrical and Electronics Engineering*. Hoboken, NJ, USA: Wiley, 1999.

[33] B. E. Saleh and M. C. Teich, *Fundamentals of Photonics*. New York, NY, USA: Wiley, 2019.

[34] S. Mirjalili, "SCA: A sine cosine algorithm for solving optimization problems," *Knowl. Based Syst.*, vol. 96, pp. 120–133, Mar. 2016.

[35] J.-B. Wang, Q.-S. Hu, J. Wang, M. Chen, and J.-Y. Wang, "Tight bounds on channel capacity for dimmable visible light communications," *J. Light. Technol.*, vol. 31, no. 23, pp. 3771–3779, Dec. 2013.

[36] J. Li, C.-H. Wen, S. Gauza, R. Lu, and S.-T. Wu, "Refractive indices of liquid crystals for display applications," *J. Display Technol.*, vol. 1, no. 1, p. 51, Sep. 2005.

[37] X. Zhang, Q. Gao, C. Gong, and Z. Xu, "User grouping and power allocation for NOMA visible light communication multi-cell networks," *IEEE Commun. Lett.*, vol. 21, no. 4, pp. 777–780, Apr. 2017.

[38] T. Shen, V. Yachongka, Y. Hama, and H. Ochiai, "Secrecy design of indoor visible light communication network under downlink NOMA transmission," Apr. 2023, *arXiv:2304.08458*.

[39] O. Maraqa, A. S. Rajasekaran,S. Al-Ahmadi, H. Yanikomeroglu, and S. M. Sait, "A survey of rate-optimal power domain NOMA with enabling technologies of future wireless networks," *IEEE Commun. Surveys Tuts.*, vol. 22, no. 4, pp. 2192–2235, Fourthquarter 2020.

[40] O. Maraqa, U. F. Siddiqi, S. Al-Ahmadi, and S. M. Sait, "On the achievable max-min user rates in multi-carrier centralized NOMA-VLC networks," *Sensors*, vol. 21, no. 11, May 2021, Art. no. 3705.

[41] S. Aboagye, T. M. N. Ngatched, O. A. Dobre, and A. G. Armada, "Energy efficient subchannel and power allocation in cooperative VLC systems," *IEEE Commun. Lett.*, vol. 25, no. 6, pp. 1935–1939, Jun. 2021.

[42] L. Zhan, H. Zhao, W. Zhang, and J. Lin, "An optimal scheme for the number of mirrors in vehicular visible light communication via mirror array-based intelligent reflecting surfaces," *Photonics*, vol. 9, no. 3, Feb. 2022, Art. no. 129.

[43] S. Ma, T. Zhang, S. Lu, H. Li, Z. Wu, and S. Li, "Energy efficiency of SISO and MISO in visible light communication systems," *J. Light. Technol.*, vol. 36, no. 12, pp. 2499–2509, Jun. 2018.

[44] Y. Liu, X. Mu, X. Liu, M. Di Renzo, Z. Ding, and R. Schober, "Reconfigurable intelligent surface-aided multi-user networks: Interplay between NOMA and RIS," *IEEE Wireless Commun.*, vol. 29, no. 2, pp. 169–176, Apr. 2022.